TITLE

Conditioned medium of human mesenchymal stem cells affects stem cell senescence in osteoporosis

AUTHORS

Liu Kehong[a], Kiyoshi Sakai[b], Junna Watanabe[b], Dong Jiao[a,c], Hiroshi Maruyama[a], Xinheng Li[a] , Hideharu Hibi[a,b]

[a] Department of Oral and Maxillofacial Surgery, Nagoya University Graduate School of Medicine, Nagoya, Aichi, Japan

[b] Department of Oral and Maxillofacial Surgery, Nagoya University Hospital, Nagoya, Aichi, Japan

[c] Lung Bioengineering and Regeneration, Department of Experimental Medical Sciences, Faculty of Medicine, Lund University, Lund, Sweden

Corresponding author: Kiyoshi Sakai, 65 Tsurumai-cho, Showa-Ku, Nagoya 466-8550, Japan.
Phone: +81-52-744-2348, **E-mail**: www-kiyo@med.nagoya-u.ac.jp (K. Sakai).

ABSTRACT

Systemic transplantation of mesenchymal stem cells (MSCs) and conditioned medium derived from MSCs have been reported to recover bone loss in animal models of osteoporosis; however, the underlying mechanisms remain unclear. We recently reported that extracellular vesicles released from human mesenchymal stem cells (hMSCs) prevent senescence of stem cells in bisphosphonate-related osteonecrosis of the jaw model. In this study, we aimed to compare the effects of conditioned medium (hMSCs-CM) from early and late passage hMSCs on cellular senescence and to verify the benefits of CM from early passage hMSCs in mitigating the progression of osteoporosis through the prevention of cellular senescence. We investigated the distinct endocrine effects of early (P5) and late (P17) passage hMSCs in vitro, as well as the preventive benefits of early passage hMSCs-CM in osteoporosis model triggered by ovariectomy. Our results indicate that long-term cultured hMSCs contributed to the progression of inflammatory transcriptional programs in P5 hMSCs, ultimately impairing their functionality and enhancing senescence-related characteristics. Conversely, early passage hMSCs reversed these alterations. Moreover, early passage hMSCs-CM infused intravenously in a postmenopausal osteoporosis mouse model suppressed bone degeneration and prevented osteoporosis by reducing ovariectomy-induced senescence in bone marrow MSCs and reducing the expression of senescence-associated secretory phenotype-related cytokines. Our findings highlight the high translational value of early passage hMSCs-CM in antiaging intervention and osteoporosis prevention.

Keywords:

postmenopausal osteoporosis, human mesenchymal stem cells, conditioned medium, cellular senescence, DNA damage response

1. Introduction

Osteoporosis tends to cause severe fractures in elderly patients. Investigation of the molecular mechanisms that underlie osteoporosis and the development of efficacious preventative and therapeutic approaches hold great significance for human health [1-3]. In this context, human clinical trials and preclinical animal studies have been undertaken to explore novel treatments and innovative prevention methods for osteoporosis [4, 5].Instudies focusing on preventation methods for osteoporosis, mesenchymal stem cells (MSCs) transplantation has gained significant attention due to its remarkable outcomes[6-8]. Furthermore, the conditioned medium of MSCs (MSCs-CM) achieves a similar therapeutic effect, as does stem cell transplantation. Recent studies have also shown that MSCs-CM affects tissue repair, such as in neural tissue regeneration [9], skin wound healing [10], and bone defect [11], through stem cell signaling. In particular, evidence exists for the cell signaling of MSCs in promoting bone regeneration through a variety of mechanisms, including adjustment of the balance between osteogenesis and bone resorption [12,13], alteration in the direction of MSCs differentiation toward osteogenesis rather than lipogenesis [14,15], and attenuation of apoptosis [16]. The use of MSCs-CM circumvents the complications associated with stem cell transplantation, including carcinogenesis, robust immune responses, and difficulties in ensuring a consistent cell supply [17,18]. However, the precise mechanism behind restoring recipient bone marrow MSCs function in the MSCs-CM therapy remains incompletely understood.

Cellular senescence, a basic aging mechanism, plays an important role in physiological growth responses and pathological development of diseases [19, 20]. Inhibition of senescence-associated secretory phenotype (SASP) or elimination of senescent cells has been shown to have preventative and therapeutic effects on diseases by an increasing number of researchers [21-23]. Our group previously demonstrated that in a mouse model of mandibular salivary gland injury generated using X-ray radiation, stem cells inhibited cellular senescence in alveolar epithelial cells through stem cell signaling mediated by extracellular vehicles (EVs) [24]. Moreover, in the bisphosphonate-related osteonecrosis of the jaw model, extracellular vesicles prevented senescence of stem cells, osteoblasts, and fibroblasts, reduced inflammation, and accelerated wound healing. This complex mechanism prevented by suppressing cellular senescence in drug-induced osteonecrosis of the jaw via stem cell-mediated signaling [25]. In addition, cellular senescence is closely associated with the development of bone and osteoarticular diseases. The clearance of senescent cells benefits cartilage regeneration and can reduce age-related bone loss [26, 27]. Recent studies highlight that the application of MSCs and MSCs-based (cell and cell-free) therapies effectively prevents stem cells from aging and exhaustion, which has become a novel strategy against age-related disorders [28]. However, few studies have focused on examining the effect of MSCs-CM on cellular senescence in a model of postmenopausal osteoporosis.

We hypothesized that a CM of human bone marrow-derived MSCs (hMSCs-CM) would prevent postmenopausal osteoporosis development by inhibiting stem cells from entering a senescence state through endocrine effects. To test this hypothesis, we performed an in vitro study in

which early (P5) and late (P17) passage hMSCs were treated with CM of P17 and P5 hMSCs, respectively. We also generated a postmenopausal osteoporosis mouse model and treated it with hMSCs-CM. The different effects of CMs from early and late passage hMSCs on cellular senescence were determined in vitro. We also examined the changes in bone microstructure and the production of biochemical markers of senescence following hMSCs-CM treatment.

2. Materials and methods

2.1. Cell culture and conditioned medium (CM) generation

hMSCs were purchased from Lonza (PT-2501) and cultured in Dulbecco's modified Eagle medium (DMEM; Sigma-Aldrich, USA) supplemented with 10% fetal bovine serum (GE Healthcare Bioscience, Little Chalfont, UK)), and 1% antibiotic-antimycotic (Invitrogen, Carlsbad, CA) at 37°C in a 5% CO_2 incubator. The culture medium was changed every 3 days. We obtained comparably senescent (passage 17, P17) cells through serial passage. We used the earlier passaged (passage 5, P5) and P17 cells for the experiments. To collect P5 and P17 CM, P5 and P17 cells were cultured until they were 80% confluent, after which the culture medium was replaced with serum-free DMEM. Cells were incubated for an additional 48 h, and CM was harvested as described previously [29].

2.2. Measurement of cell proliferation

hMSCs (5×10^3 cells per well) were plated in 96-well plates and incubated in complete medium with DMEM, P5 CM, or P17 CM. The cells were cultured for 2 h in fresh complete medium with CCK-8 reagent (Cell counting Kit-8, Dojindo, Japan) every 24 h for 7 days. The optical density (OD) at 450 nm was measured using a microplate reader (Infinite 200 PRO, Tecan, Japan). The CCK-8 solution was also added to four wells without cells, which served as the blank group. A curve was plotted based on the OD values. The experiment was repeated three times for each group.

2.3. Osteoblast differentiation and quantification

When the cells reached 90% confluence after 96 h of treatment with DMEM, P5 CM, or P17 CM, the culture medium was changed with an osteogenic induction medium. Osteoblast differentiation was induced using an osteogenic induction medium that consisted of DMEM (Sigma-Aldrich) supplemented with 10% FBS, 100 IU/mL penicillin, 100 mg/mL streptomycin, 50 μM ascorbate-2-phosphate (Sigma-Aldrich), 10 mM β-glycerophosphate (Sigma-Aldrich), and 0.1 μM dexamethasone. The medium was changed every 3 days. After 21 days of cultivation, the cells were fixed with ethanol (EtOH) for 15 min and stained with Alizarin red S (40 mM, pH 4.2, Sigma-Aldrich). The staining intensity was quantified as described previously [30].

2.4. Quantification of senescent cells

hMSCs (2.5×10^4 cells per well) were cultured on 8-well chamber slides (Thermo Fisher Scientific) after treatment with DMEM, P5 CM, or P17 CM for 96 h. The cells were fixed with 4% paraformaldehyde for 20 min at RT (20°C-22°C) and then incubated overnight with the SA-β-Gal (SPiDER-β-Gal, Dojindo, Japan) staining solution (pH = 6.0) to evaluate the senescence-associated β-galactosidase (SA-β-Gal) activity. Thereafter, nuclei were stained with DAPI (NucBlue™, Thermo Fisher) and images (n = 12 per group) were acquired at a 20-fold magnification with a

fluorescence microscope, BZ-X800 (Keyence, Japan). To detect the SA-β-Gal activity in the bone tissue, 4 μm coronal sections were prepared using the Kawamoto method [31]. The sections were stained according to the manufacturer's instructions and mounted with a mounting medium containing DAPI (VECTASHIELD Hard, Vector Laboratories). A confocal laser scanning microscope (A1Rsi, Nikon, Japan) was used to observe the samples at a 100-fold magnification (n = 10 per group). Cells exhibiting green signal in the cytosol were counted as positive. The proportion of SA-β-Gal-positive cells was calculated using the QuPath software.

2.5. Quantitative real-time polymerase chain reaction (RT-qPCR)

hMSCs (5×10^5 cells per well) were cultured in 100 mm dishes (Thermo Fisher Scientific), after treatment with DMEM, P5 CM, or P17 CM for 96 h. RNA was extracted from the cells with TRIzol reagent (Thermo Fisher Scientific) according to the manufacturer's protocol. For *in vivo* analysis, the distal epiphysis of the femur was flash-frozen in liquid nitrogen, crushed with a disposable homogenizer (BioMasher II, Nippi, Japan), and then used for the extraction of total RNA with TRIzol. A spectrophotometer was used to quantify total RNA levels. The RNA integrity was checked on a 1% agarose gel. Reverse transcription was performed with Superscript IV reverse transcriptase (Thermo Fisher Scientific) using 0.5 μg total RNA in a 20 μL reaction volume. RT-qPCR was performed using THUNDERBIRD SYBR qPCR Mix (Toyobo, Osaka, Japan) on a real-time PCR system (Agilent Technologies, Tokyo, Japan). The specific primers were designed using Primer 3 (Supplementary Table 1, 2). Results for the SASP (including IL-6, MMP2, IL-1β, PAI-1, MCP-1, and TNF-α) and genes related to cell cycle arrest in senescence ($p16^{INK4a}$, p21, and p53) were normalized against glyceraldehyde 3-phosphate dehydrogenase (GAPDH). The results of relative telomere length were normalized against cyclin-dependent kinase 4 inhibitor b (36B4), based on the Cawthon method [32]. Changes in the gene expression were calculated relative to the control.

2.6. Osteoporosis models and CM treatments

All animal experiments were approved by the Institutional Animal Care and Use Committee of Nagoya University (Approval Number: M210759-002, M210183-001, and M220136-001). Sixty-four female C57BL/6J mice (9-week-old) were purchased from CLEA Japan, Inc. (Tokyo, Japan). The postmenopausal osteoporotic mouse model was generated by bilateral ovariectomy (OVX) [33]. These mice were randomly divided into four groups (n = 10 per group): (1) Control: without any surgeries or injections; (2) Sham: bilateral ovaries exposure without any damage to the ovary tissue; (3) OVX + DMEM: OVX mice were injected with 500 μL of DMEM via the tail vein once a week starting the week of surgery; and (4) OVX + CM: 500 μL of P5 CM was injected intravenously at the same timing as above. The body weight of mice was recorded every two weeks. Four months after the establishment of the OVX model, the mice were anesthetized, and micro-CT scans of their right femur and lumbar spines (L5) were taken for further analysis. After the mice were euthanized, RNA from their right femur was extracted and subjected to RT-qPCR analysis. The left femur was separated and used for SA-β-Gal and immunofluorescence assays. The uterus of mice was extracted, weighed, and stored in a 4% paraformaldehyde solution.

2.7. μCT Imaging

Representative images of the lumbar spine (L5) and distal femoral metaphysis were generated with

a 3D reconstruction software program (NRecon and CTVox, Bruker). Quantitative analyses of the distal femoral and lumbar spine (L5) metaphyses were performed using an 1176 micro-computed tomography (μCT) system (Skyscan, Bruker, Billerica, MA) with the following parameters: 50 kV, 500 mA, high resolution, Al 0.5 mm, and 9 μm voxel size.

For both the vertebral trabecular region and femoral trabecular region, we evaluated 100 transverse μCT slices between the 50th slice located underneath the growth plate and caudal end plate. For femoral cortical regions, we evaluated 100 transverse μCT slices between the 400th slice located underneath the growth plate and caudal end plate. 3D structural parameters included trabecular bone volume fraction (Tb.BV/TV; %), trabecular number (Tb.N; 1/mm), trabecular thickness (Tb.Th; mm), trabecular separation (Tb.Sp; mm), bone mineral density (BMD; mg/cm3), and cortical thickness (Ct.Th; μm). Density values were calibrated using hydroxyapatite phantoms with BMD values of 0.25 and 0.75 g/cm^3 (Skyscan). The imaging settings and thresholds of μCT were maintained consistent throughout all analyses. Two blinded investigators performed all measurements.

2.8. Immunofluorescence staining

Immunofluorescence staining was conducted following the manufacturer's instructions. Tissue sections (4 μm coronal sections, Kawamoto) were fixed for 2 min with 4% paraformaldehyde and then dehydrated for 2 min with 100% ethanol. The sections were subsequently permeabilized with 0.1% Triton X-100 for 10 min and blocked with 3% bovine serum albumin for 1 h. They were then incubated overnight with a primary antibody, anti-Nestin (ab134017, Abcam) or phospho-histone H2A.X antibody (2577, Cell Signaling Technology, Danvers, MA, USA). After washing, the sections were incubated with a secondary antibody, goat anti-chicken Alexa Fluor 594 (ab1613906, Abcam) or donkey anti-rabbit Alexa Fluor 488 (ab1608521, Abcam), for 2 h at room temperature. After a second round of washing, the slices were mounted with a mounting medium containing DAPI. The sections were observed using a confocal laser scanning microscope (A1Rsi, Nikon, Japan) at 100-fold magnification (n = 10 per group). The cells exhibiting a green signal in the nuclei were counted as pH2A.X-positive whereas those exhibiting green signals in the nuclei and red signals in the cytosol were counted as pH2A.X- and Nestin-positive cells. The proportions of pH2A.X-positive cells and the ratio of pH2A.X- and Nestin-positive cells were calculated using the QuPath software.

2.9. Statistical analyses

All data are presented as mean ± standard deviation of values from at least three independent experiments. Statistical analysis was performed using GraphPad Prism 9 version 9.0.0.
Student's t-test was used to determine the p-value. Multiple comparison post-tests were combined with one-way analysis of variance to determine differences between groups. Differences were considered statistically significant at $p < 0.05$.

3. Results

3.1. Senescent hMSCs impair cell function, whereas young hMSCs partially improve cell function, via endocrine effects

After long-term in vitro culture, hMSCs in passage 17 (P17 hMSCs) showed signs of aging [34], which included decreased cell proliferation and osteogenic differentiation capacity compared

with those of passage 5 hMSCs (P5 hMSCs) from the same donors. The markers of cellular senescence in P17 hMSCs, including the SA-β-Gal activity and expression levels of genes related to cell cycle arrest in senescence and SASP genes, exhibited an increase. Similarly, the relative length of telomere in P17 hMSCs was shortened compared with that in P5 hMSCs. These results indicate that, after a long-term in vitro cell culture, P17 hMSCs are in a more aged state compared with P5 hMSCs. (Fig. S1A-E) In subsequent experiments, we considered P5 cells as young stem cells and P17 cells as senescent stem cells, and CM from P5 cells as young CM and that from P17 cells as senescent CM. After culture with DMEM or P17 CM for 96 h, P5 hMSCs treated with senescent CM exhibited a lower cell proliferation capacity than P5 hMSCs treated with DMEM (Fig. 1B). However, treatment with P5 CM for 96 h did not have any noteworthy effect on the proliferation ability of P17 hMSCs (Fig. 1C). Alizarin red S staining and quantification of the staining intensity showed a statistically significant reduction in calcium deposits in P17 CM-treated P5 hMSCs over a 3-week culture in osteogenic-induction medium. There was a significant increase in the levels of calcium deposits in P17 hMSCs treated with P5 CM after 3 weeks of culture (Fig. 1D, E). Collectively, these findings indicate that senescent hMSCs have the potential to negatively affect cellular function via endocrine effects whereas young hMSCs possess the ability to restore cellular function partially through endocrine effects.

3.2. Senescent hMSCs facilitate, whereas young hMSCs prevent, cellular senescence through endocrine effects

To examine the impact of the endocrine effects of P5 and P17 hMSCs on cellular senescence, we performed SA-β-Gal staining and RT-qPCR analysis to evaluate the expression of genes related to cellular senescence in P5 cells following treatment with P17 CM, as well as in P17 cells following treatment with P5 CM. P5 cells exhibited a notable increase in the SA-β-Gal activity in the P17 CM-treated group, compared with that in the DMEM-treated group. In contrast, P17 cells treated with P5 CM showed a reduction in the SA-β-Gal activity compared with P17 cells treated with DMEM (Fig. 2A, B). The RT-qPCR results indicated a modest increase in the expression levels of several SASP factors (IL6 and MCP-1) in P5 cells treated with P17 CM compared with the levels in P5 cells treated with DMEM. Furthermore, no changes in the expression of genes related to cell cycle arrest in senescence ($p16^{INK4a}$, p21, and p53) were noted between the two groups, and the P17 CM treatment did not have any obvious effect on the telomere length (Fig. 2C, D). On the contrary, P5 CM-treated P17 cells exhibited a reduction in the expression levels of SASP factors (IL8 and PAI-1) and a slight reduction in the expression of the cell cycle inhibitory kinase gene (p53). Besides, treatment with P5 CM resulted in a slight elongation in the telomere length (Fig. 2E, F). These findings suggest that treatment with P17 CM leads to the manifestation of senescent characteristics in young hMSCs, whereas P5 CM alleviates certain senescence-related phenotypes in senescent hMSCs.

3.3. hMSCs-CM prevented bone loss in osteoporosis

To explore the effects of early passage hMSCs-CM on primary osteoporosis, we established an animal model of OVX-induced postmenopausal osteoporosis [33]. CM, or an equal volume of vehicle (DMEM), was intravenously administrated to osteoporotic mice. A sham surgery group (Sham) was included to rule out the effect of OVX on the experimental findings. After OVX, a notable rise in total body weight was detected in OVX mice when compared to the Control and Sham mice. The size and weight of the uterus in OVX mice were significantly decreased compared with those in Control and Sham mice (Fig. S2A, B), indicating the success of OVX. Micro-CT 3D

imaging analyses was conducted on the distal femur and L5 for Control, Sham, OVX + DMEM, and OVX + CM mice. CT scanning of the femur revealed that DMEM-treated OVX mice had decreased trabecular bone mass in the femur compared with Control and Sham mice, whereas intravenous administration of CM to OVX mice for 4 months prevented bone loss (Fig. 3B). Quantification of bone parameters showed that Tb.BV/TV, Tb.Th, Tb.N, and BMD values in DMEM-treated OVX mice were significantly lower than those in the Control and Sham groups, whereas all four down-regulated parameters induced by OVX were restored after CM treatment (Fig. 3C-F). Trabecular separation in OVX mice was increased compared with that in Control and Sham mice, and this reduction was reversed by CM treatment (Fig. 3G). CT analyses of L5 demonstrated similar improvements with CM administration in the trabecular bone at the vertebra. Compared with DMEM-treated mice, CM-treated mice exhibited a better spine trabecular bone microarchitecture (Fig. 3H). The levels of Tb.BV/TV, Tb.Th, Tb.N, and BMD in the OVX + DMEM group were significantly lower than those in Control and Sham groups. However, all four of these OVX-induced changes were ameliorated by CM treatment (Fig. 3I-L). Similarly, treatment with CM decreased the enhanced trabecular separation observed in OVX mice compared with that in Control and Sham mice (Fig. 3M). All these results suggest that CM can prevent the loss of bone mass in postmenopausal osteoporotic mice.

3.4. hMSCs-CM reduces cellular senescence in the bone microenvironment by preventing bone marrow MSCs from entering a senescent state

The number of X-Gal-positive cells was increased close to the growth plate (Fig. S4A, B). We conducted a more detailed examination of the bone microenvironment around the growth plate and performed immunofluorescence staining of the distal femur. A notable increase in the percentage of SA-β-Gal-positive cells was observed after ovariectomy compared with that in the Control and Sham mice. The administration of CM for four months effectively mitigated the increase in the percentage of SA-β-Gal-positive cells, consistent with the results of X-Gal staining (Fig. 4A, C). pH2A.X is a representative protein that is highly expressed during the DNA damage response and Nestin is a protein that labels MSCs. Based on the results of double staining for Nestin with pH2A.X, bone marrow MSCs in the bone microarchitecture from the OVX + DMEM mice exhibited DNA damage phenotypes, which affected the cellular senescence of the surrounding non-stem cells, increasing the rate of pH2A.X-positive cells. In contrast, systemic injection of CM prevented the DNA damage in bone marrow MSCs and the increase in the percentage of pH2A.X-positive cells in the femur (Fig. 4B, D, E). Furthermore, the expression levels of aging-related genes in the distal femur of mice were evaluated. The expression of SASP factors (IL-6, MMP2, IL-1β, PAI-1, MCP-1, and TNF-α) and genes related to cell cycle arrest in senescence (p16INK4a, p21, and p53) were elevated in the OVX + DMEM group. The injection of CM significantly reduced the expression of senescence and inflammatory cytokines genes (Fig. 4F). Similarly, the changes in telomere length showed that CM injection rescued telomere length shortage caused by ovariectomy (Fig. 4G).

4. Discussion

In the present study, we show that hMSC-CM prevented the bone loss in osteoporosis by inhibiting the cellular senescence of bone marrow MSCs. Specifically, in vitro, senescent CM (P17 CM)-treated P5 cells exhibited decreased proliferation capacity, reduced osteogenic differentiation capacity, increased SA-β-Gal activity, and increased SASP expression levels, and exhibited typical features of an early stage of cellular senescence. In contrast, P17 cells treated with young CM (P5 CM, subsequently used in vivo) exhibited the opposite changes. In vivo, hMSCs-CM administration

effectively interrupted cellular senescence and prevented osteoporosis-related bone loss.

This study unravels a connection between the endocrine effects of stem cells and cellular senescence. Previous research has shown that hMSCs-CM can effectively function as a novel and reliable preventative medication for osteoporosis. However, the mechanism behind this effect is not yet completely understood [17]. According to our results, after 96 h of cultivation with P17 CM, the proliferative ability of P5 cells was partially reduced rather than completely suppressed. Besides, the SA-β-Gal activity and the expression levels of IL6 and MCP-1 were increased. No significant changes were observed in the expression levels of cell cycle kinases ($p16^{INK4a}$, p21, and p53) and relative length of telomere. These findings suggest that hMSCs in the senescence state can induce nearby cells to enter a presenescent state by creating an inflammatory environment [34]. On the contrary, the proliferation ability of P17 cells was not improved after 96 h of culture with P5 CM, which suggests that ultimately proliferation arrest of P17 hMSCs could not be repaired with P5 CM treatment [35]. In addition, P5 CM effectively suppressed the SA-β-Gal activity, attenuating SASP (IL8 and PAI-1) expression, causing a slight downregulation of p53 expression (no significant changes were observed for $p16^{INK4a}$ and p21), and resulting in a modest increase in the telomere length in P17 cells. This reduction in senescence characteristics by short-term P5 CM treatment was probably through the suppression of p53 activation. Long-term P5 CM treatment may rescue the chronic inflammatory environment created by senescent cells. As a result, these lasting beneficial effects of P5 CM may prevent the accumulation of cellular senescence in an in vivo environment which is identical to the results observed in our vivo qPCR analysis. However, all the above interpretations are based on in vitro results obtained via culture with CMs for 96 h. Future analysis will focus on long-term experiments. Moreover, experiments to search specific effectors of P5 CM and the possible signal pathway are needed in the future.

Postmenopausal osteoporosis is classified as primary osteoporosis and is characterized by marked bone reduction via hyperactivated osteoclast activity, which subsequently increases the susceptibility to fragility fractures. However, the detailed mechanisms underlying the estrogen-deficient condition are not fully understood [36]. Previous studies have shown that estrogen deficiency increases DNA methylation and downregulates telomerase activity in postmenopausal women and ovariectomized animals [37, 38]. Senescence is related to DNA demethylation and reduction in the telomerase activity [39, 40]. Here, we demonstrate cellular senescence by OVX in the postmenopausal osteoporosis model for the first time. We observed that estrogen deficiency triggered the senescence of bone marrow MSCs and surrounding cells in the stem cell niche. However, the direct inducement for double DNA strand breaks caused by estrogen deficiency is still unclear. Furthermore, despite choosing the stem cell niches adjacent to the growth plate [41], where MSCs are likely to be concentrated, the results revealed a limited number of Nestin-positive cells within the observed regions. This small number may be related to the extremely low percentage of MSCs in the bone marrow environment, which is approximately 0.01% [42]. We also confirmed the accumulation of IL-6, MMP2, IL-1β, PAI-1, MCP-1, and TNF-α in SASP after OVX, which suggests that there was a chronic inflammation environment in OVX-induced osteoporosis. It is reasonable to believe that persistent inflammatory stimuli could increase oxidative stress within the bone microenvironment, leading to DNA damage [43]. A deeper examination of this assumption will be undertaken in future research.

As for our osteoporotic mice, we also found that estrogen reduction did not severely affect the femoral cortical bone (there was a slight decrease in cortical bone thickness but no significant

change in BMD, and CM treatment had no specific effect on the uninjured cortical bone (Fig. S3A-C)). The time point of CT for animal studies was 4 months after the OVX, which corresponds to the early stage of osteoporosis development in clinical postmenopausal osteoporosis patients [44], where estrogen deficiency has not yet fully affected the cortical bone of the thigh bone diaphysis.

Our results confirm that the early pathogenic mechanism in OVX-induced postmenopausal osteoporosis is related to cellular senescence. This study also offers a new strategy to prevent postmenopausal osteoporosis by administration of CM to protect bone marrow MSCs from entering a stage of senescence.

Author Contributions

Kehong Liu: Investigation (lead); methodology (lead); formal analysis (lead); writing – original draft (lead); **Kiyoshi Sakai**: Conceptualization (lead); writing – review and editing (lead); funding (lead); **Junna Watanabe**: Methodology (equal); formal analysis (supporting); funding (lead); **Dong Jiao**: Methodology (supporting); writing – review and editing (supporting); **Hiroshi Maruyama**: Formal analysis (equal); writing – review and editing (equal); **Xinheng Li**: Methodology (supporting); formal analysis (supporting); **Hideharu Hibi**: Conceptualization (supporting); writing – original draft (supporting); writing – review and editing (supporting).

Study approval

All animal procedures were conducted in accordance with the National Institutes of Health Guidelines for the Care and Use of Laboratory Animals and were approved by the Nagoya University School of Medicine Animal Care and Use Committee (M210759-002, M210183-001, and M220136-001)

Funding

This work was supported by JSPS KAKENHI (Grant Numbers: 22K10215, 21K10067, 21K17134, 20K23075).

Acknowledgments

We thank Yoshiro Koma, Nobutomo Uejima, Satoshi Yamaguchi, Masahito Fujio, Xinman Song, Qi Chang, Hui Chen, and Huiting Bian from the Department of Oral and Maxillofacial Surgery for their comments and support for this study. We also wish to acknowledge the Division for Medical Research Engineering, Nagoya University Graduate School of Medicine, for support with the confocal laser scanning microscopy, using the micro-computed tomography system Skyscan 1176, analysis using the 3D reconstruction software program, and other help.

Reference

[1] J.E. Compston, M.R. McClung, W.D. Leslie, Osteoporosis, Lancet. 393 (2019) 364–376. https://doi.org/10.1016/S0140-6736(18)32112-3.

[2] F. Cosman, S.J. de Beur, M.S. LeBoff, E.M. Lewiecki, B. Tanner, S. Randall, R. Lindsay, National Osteoporosis

Foundation, Clinician's guide to prevention and treatment of osteoporosis, Osteoporos. Int. 25 (2014) 2359–2381. https://doi.org/10.1007/s00198-014-2794-2.

[3] D.H. Solomon, L. Rekedal, S.M. Cadarette, Osteoporosis treatments and adverse events, Curr. Opin. Rheumatol. 21 (2009) 363–368. https://doi.org/10.1097/BOR.0b013e32832ca433.

[4] Tella SH, Gallagher JC, Prevention and treatment of postmenopausal osteoporosis. The Journal of Steroid Biochemistry and Molecular Biology. 2014;142(0960-0760):155-170. https://doi.org/10.1016/j.jsbmb.2013.09.008.

[5] Liang, B., Burley, G., Lin, S, Osteoporosis pathogenesis and treatment: existing and emerging avenues. Cell Mol Biol Lett **27**, 72 (2022). https://doi.org/10.1186/s11658-022-00371-3.

[6] Infante A, Gener B, Vázquez M, et al. Reiterative infusions of MSCs improve pediatric osteogenesis imperfecta eliciting a pro-osteogenic paracrine response: TERCELOI clinical trial. *Clinical and Translational Medicine*. 2021;11(1):e265. https://doi.org/10.1002/ctm2.265.

[7] Golpanian S, DiFede DL, Khan A, et al. Allogeneic Human Mesenchymal Stem Cell Infusions for Aging Frailty. *The Journals of Gerontology: Series A*. 2017;72(11):1505-1512. https://doi.org/10.1093/gerona/glx056.

[8] Götherström C, Westgren M, Shaw SWS, et al. Pre- and Postnatal Transplantation of Fetal Mesenchymal Stem Cells in Osteogenesis Imperfecta: A Two-Center Experience. *STEM CELLS Translational Medicine*. 2013;3(2):255-264. https://doi.org/10.5966/sctm.2013-0090.

[9] K.B. Gama, D.S. Santos, A.F. Evangelista, D.N. Silva, A.C. de Alcântara, R.R. Dos Santos, M.B.P. Soares, C.F. Villarreal, Conditioned Medium of Bone Marrow-Derived Mesenchymal Stromal Cells as a Therapeutic Approach to Neuropathic Pain: A Preclinical Evaluation, Stem Cells Int. 2018 (2018) 8179013. https://doi.org/10.1155/2018/8179013.

[10] M.N.M. Walter, K.T. Wright, H.R. Fuller, S. MacNeil, W.E.B. Johnson, Mesenchymal stem cell-conditioned medium accelerates skin wound healing: An in vitro study of fibroblast and keratinocyte scratch assays, Exp. Cell Res. 316 (2010) 1271–1281. https://doi.org/10.1016/j.yexcr.2010.02.026.

[11] M. Osugi, W. Katagiri, R. Yoshimi, T. Inukai, H. Hibi, M. Ueda, Conditioned media from mesenchymal stem cells enhanced bone regeneration in rat calvarial bone defects, Tissue Eng. Part A. 18 (2012) 1479–1489. https://doi.org/10.1089/ten.TEA.2011.0325.

[12] Y. Qin, L. Wang, Z. Gao, G. Chen, C. Zhang, Bone marrow stromal/stem cell-derived extracellular vesicles regulate osteoblast activity and differentiation in vitro and promote bone regeneration in vivo, Sci. Rep. 6 (2016) 21961. https://doi.org/10.1038/srep21961.

[13] X. Yang, J. Yang, P. Lei, T. Wen, LncRNA MALAT1 shuttled by bone marrow-derived mesenchymal stem cells-secreted exosomes alleviates osteoporosis through mediating microRNA-34c/SATB2 axis, Aging. 11 (2019) 8777–8791. https://doi.org/10.18632/aging.102264.

[14] Y.H. Kim, M. Park, K.A. Cho, B.K. Kim, J.H. Ryu, S.Y. Woo, K.H. Ryu, Tonsil-derived mesenchymal stem cells promote bone mineralization and reduce marrow and visceral adiposity in a mouse model of senile osteoporosis, Stem Cells Dev. 25 (2016) 1161–1171. https://doi.org/10.1089/scd.2016.0063.

[15] Y. Hu, Y. Zhang, C.Y. Ni, C.Y. Chen, S.S. Rao, H. Yin, J. Huang, Y.J. Tan, Z.X. Wang, J. Cao, Z.Z. Liu, P.L. Xie, B. Wu, J. Luo, H. Xie, Human umbilical cord mesenchymal stromal cells-derived extracellular vesicles exert potent bone protective effects by CLEC11A-mediated regulation of bone metabolism, Theranostics. 10 (2020) 2293–2308. https://doi.org/10.7150/thno.39238.

[16] R. Saleem, S. Mohamed-Ahmed, R. Elnour, E. Berggreen, K. Mustafa, N. Al-Sharabi, Conditioned medium from bone marrow mesenchymal stem cells restored oxidative stress-related impaired osteogenic differentiation, Int. J. Mol. Sci. 22 (2021) 13458. https://doi.org/10.3390/ijms222413458.

[17] X. Liang, Y. Ding, Y. Zhang, H.F. Tse, Q. Lian, Paracrine mechanisms of mesenchymal stem cell-based therapy:

Current status and perspectives, Cell Transplant. 23 (2014) 1045–1059. https://doi.org/10.3727/096368913X667709.

[18] F.J. Vizoso, N. Eiro, S. Cid, J. Schneider, R. Perez-Fernandez, Mesenchymal stem cell secretome: Toward cell-free therapeutic strategies in regenerative medicine, Int. J. Mol. Sci. 18 (2017) 1852. https://doi.org/10.3390/ijms18091852.

[19] W. Huang, L.J. Hickson, A. Eirin, J.L. Kirkland, L.O. Lerman, Cellular senescence: The good, the bad and the unknown, Nat. Rev. Nephrol. 18 (2022) 611–627. https://doi.org/10.1038/s41581-022-00601-z.

[20] T. Tchkonia, Y. Zhu, J. van Deursen, J. Campisi, J.L. Kirkland, Cellular senescence and the senescent secretory phenotype: Therapeutic opportunities, J. Clin. Invest. 123 (2013) 966–972. https://doi.org/10.1172/JCI64098.

[21] P.J. Barnes, J. Baker, L.E. Donnelly, Cellular senescence as a mechanism and target in chronic lung diseases, Am. J. Respir. Crit. Care Med. 200 (2019) 556–564. https://doi.org/10.1164/rccm.201810-1975TR.

[22] C. Amor, J. Feucht, J. Leibold, Y.J. Ho, C. Zhu, D. Alonso-Curbelo, J. Mansilla-Soto, J.A. Boyer, X. Li, T. Giavridis, A. Kulick, S. Houlihan, E. Peerschke, S.L. Friedman, V. Ponomarev, A. Piersigilli, M. Sadelain, S.W. Lowe, Senolytic CAR T cells reverse senescence-associated pathologies, Nature. 583 (2020) 127–132. https://doi.org/10.1038/s41586-020-2403-9.

[23] M. Xu, T. Tchkonia, H. Ding, M. Ogrodnik, E.R. Lubbers, T. Pirtskhalava, T.A. White, K.O. Johnson, M.B. Stout, V. Mezera, N. Giorgadze, M.D. Jensen, N.K. LeBrasseur, J.L. Kirkland, JAK inhibition alleviates the cellular senescence-associated secretory phenotype and frailty in old age, Proc. Natl Acad. Sci. U. S. A. 112 (2015) E6301–E6310. https://doi.org/10.1073/pnas.1515386112.

[24] J. Dong, K. Sakai, Y. Koma, J. Watanabe, K. Liu, H. Maruyama, K. Sakaguchi, H. Hibi, Dental pulp stem cell-derived small extracellular vesicle in irradiation-induced senescence, Biochem. Biophys. Res. Commun. 575 (2021) 28–35. https://doi.org/10.1016/j.bbrc.2021.08.046.

[25] J. Watanabe, K. Sakai, Y. Urata, N. Toyama, E. Nakamichi, H. Hibi, Extracellular vesicles of stem cells to prevent BRONJ, J. Dent. Res. 99 (2020) 552–560. https://doi.org/10.1177/0022034520906793.

[26] O.H. Jeon, C. Kim, R.M. Laberge, M. Demaria, S. Rathod, A.P. Vasserot, J.W. Chung, D.H. Kim, Y. Poon, N. David, D.J. Baker, J.M. van Deursen, J. Campisi, J.H. Elisseeff, Local clearance of senescent cells attenuates the development of post-traumatic osteoarthritis and creates a pro-regenerative environment, Nat. Med. 23 (2017) 775–781. https://doi.org/10.1038/nm.4324.

[27] J.N. Farr, M. Xu, M.M. Weivoda, D.G. Monroe, D.G. Fraser, J.L. Onken, B.A. Negley, J.G. Sfeir, M.B. Ogrodnik, C.M. Hachfeld, N.K. LeBrasseur, M.T. Drake, R.J. Pignolo, T. Pirtskhalava, T. Tchkonia, M.J. Oursler, J.L. Kirkland, S. Khosla, Targeting cellular senescence prevents age-related bone loss in mice, Nat. Med. 23 (2017) 1072–1079. https://doi.org/10.1038/nm.4385.

[28] Infante A, Rodríguez CI. Cell and Cell-Free Therapies to Counteract Human Premature and Physiological Aging: MSCs Come to Light. *Journal of Personalized Medicine*. 2021;11(10):1043. https://doi.org/10.3390/jpm11101043.

[29] T. Tsuruta, K. Sakai, J. Watanabe, W. Katagiri, H. Hibi. Dental pulp-derived stem cell conditioned medium to regenerate peripheral nerves in a novel animal model of dysphagia, PLOS ONE. 13 (2018) e0208938. https://doi.org/10.1371/journal.pone.0208938.

[30] C.A. Gregory, W.G. Gunn, A. Peister, D.J. Prockop, An Alizarin red-based assay of mineralization by adherent cells in culture: Comparison with cetylpyridinium chloride extraction, Anal. Biochem. 329 (2004) 77–84. https://doi.org/10.1016/j.ab.2004.02.002.

[31] T. Kawamoto, Use of a new adhesive film for the preparation of multi-purpose fresh-frozen sections from hard tissues, whole-animals, insects and plants, Arch. Histol. Cytol. 66 (2003) 123–143. https://doi.org/10.1679/aohc.66.123.

[32] R.M. Cawthon, Telomere measurement by quantitative PCR, Nucleic Acids Res. 30 (2002) e47. https://doi.org/10.1093/nar/30.10.e47.

[33] Danielsen CC, Mosekilde L, Svenstrup B. Cortical bone mass, composition, and mechanical properties in female rats in relation to age, long-term ovariectomy, and estrogen substitution. *Calcified Tissue International*. 1993;52(1):26-33. https://doi.org/10.1007/bf00675623.

[34] Y. Gu, T. Li, Y. Ding, L. Sun, T. Tu, W. Zhu, J. Hu, X. Sun, Changes in mesenchymal stem cells following long-term culture in vitro, Mol. Med. Rep. 13 (2016) 5207–5215. https://doi.org/10.3892/mmr.2016.5169.

[35] D. Gnani, S. Crippa, L. Della Volpe, V. Rossella, A. Conti, E. Lettera, S. Rivis, M. Ometti, G. Fraschini, M.E. Bernardo, R. Di Micco, An early-senescence state in aged mesenchymal stromal cells contributes to hematopoietic stem and progenitor cell clonogenic impairment through the activation of a pro-inflammatory program, Aging Cell. 18 (2019) e12933. https://doi.org/10.1111/acel.12933.

[36] R. Eastell, T.W. O'Neill, L.C. Hofbauer, B. Langdahl, I.R. Reid, D.T. Gold, S.R. Cummings, Postmenopausal osteoporosis, Nat. Rev. Dis. Primers. 2 (2016) 16069. https://doi.org/10.1038/nrdp.2016.69.

[37] S. Reppe, T.G. Lien, Y.H. Hsu, V.T. Gautvik, O.K. Olstad, R. Yu, H.G. Bakke, R. Lyle, M.K. Kringen, I.K. Glad, K.M. Gautvik, Distinct DNA methylation profiles in bone and blood of osteoporotic and healthy postmenopausal women, Epigenetics. 12 (2017) 674–687. https://doi.org/10.1080/15592294.2017.1345832.

[38] J. Dan, P. Rousseau, S. Hardikar, N. Veland, J. Wong, C. Autexier, T. Chen, Zscan4 inhibits maintenance DNA methylation to facilitate telomere elongation in mouse embryonic stem cells, Cell Rep. 20 (2017) 1936–1949. https://doi.org/10.1016/j.celrep.2017.07.070.

[39] J. Cen, H. Zhang, Y. Liu, M. Deng, S. Tang, W. Liu, Z. Zhang, Anti-aging effect of estrogen on telomerase activity in ovariectomised rats—Animal model for menopause, Gynecol. Endocrinol. 31 (2015) 582–585. https://doi.org/10.3109/09513590.2015.1065478.

[40] S. Victorelli, J.F. Passos, Telomeres and cell senescence – Size matters not, EBiomedicine. 21 (2017) 14–20. https://doi.org/10.1016/j.ebiom.2017.03.027.

[41] Méndez-Ferrer S, Michurina TV, Ferraro F, et al. Mesenchymal and haematopoietic stem cells form a unique bone marrow niche. *Nature*. 2010;466(7308):829-834. https://doi.org/10.1038/nature09262.

[42] Pittenger MF, Mackay AM, Beck SC, et al. Multilineage potential of adult human mesenchymal stem cells. *Science (New York, NY)*. 1999;284(5411):143-147. https://doi.org/10.1126/science.284.5411.143.

[43] M. El Assar, J. Angulo, L. Rodríguez-Mañas, Oxidative stress and vascular inflammation in aging, Free Radic. Biol. Med. 65 (2013) 380–401. https://doi.org/10.1016/j.freeradbiomed.2013.07.003.

[44] Osterhoff G, Morgan EF, Shefelbine SJ, Karim L, McNamara LM, Augat P. Bone mechanical properties and changes with osteoporosis. *Injury*. 2016;47(2):S11-S20. https://doi.org/10.1016/s0020-1383(16)47003-8.

Figures

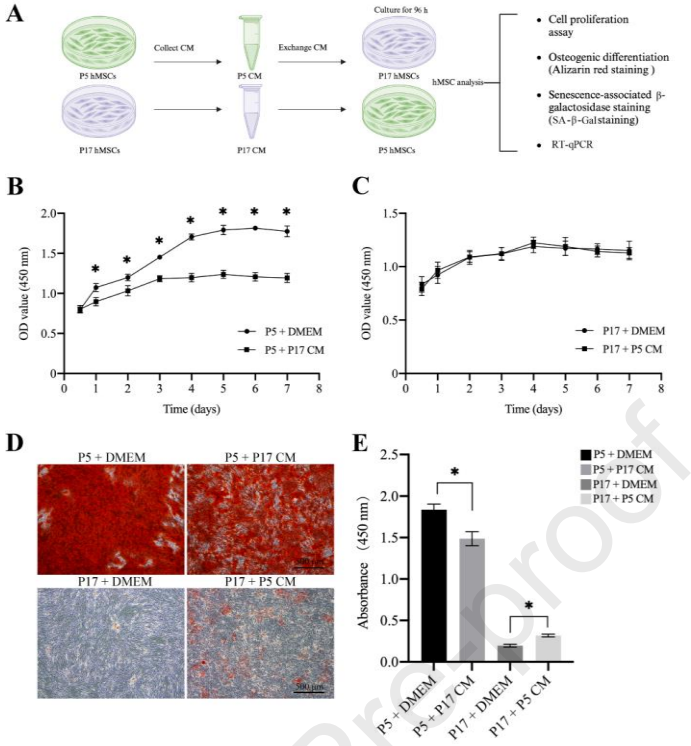

Fig. 1. Endocrine effects of young and senescent human mesenchymal stem cells (hMSCs) on essential cellular functions. (A) Schematic representation of experiments with exchange CM from young (P5) and aged (P17) hMSCs. Upon 96 h of CM culture, P5 and P17 hMSCs were analyzed for proliferation, osteogenic differentiation, senescence-associated (SA)-β-galactosidase (SA-β-Gal) staining, and gene expression. **(B, C)** After culturing with DMEM or senescent/young CM for 96 h, growth of hMSCs was determined using the Cell Counting Kit-8. **(B)** Cell proliferation was decreased over time in P5 cells treated with P17 CM ($n = 12$, $^{*}p < 0.05$ vs. DMEM-treated P5 group at 1–7 days for absorbance of WST-8 at 450 nm). **(C)** No significant difference was noted in the growth of DMEM-treated P17 cells and P5 CM-treated P17 cells ($n = 12$, $^{*}p < 0.05$ vs. DMEM-treated P17 group at 1–7 days for absorbance of WST-8 at 450 nm). **(D)** hMSCs were stained with Alizarin red S after 3 weeks of cultivation. Scale bar: 500 μm. **(E)** The staining intensity was quantified using the graph ($n = 9$, $^{*}p < 0.05$).

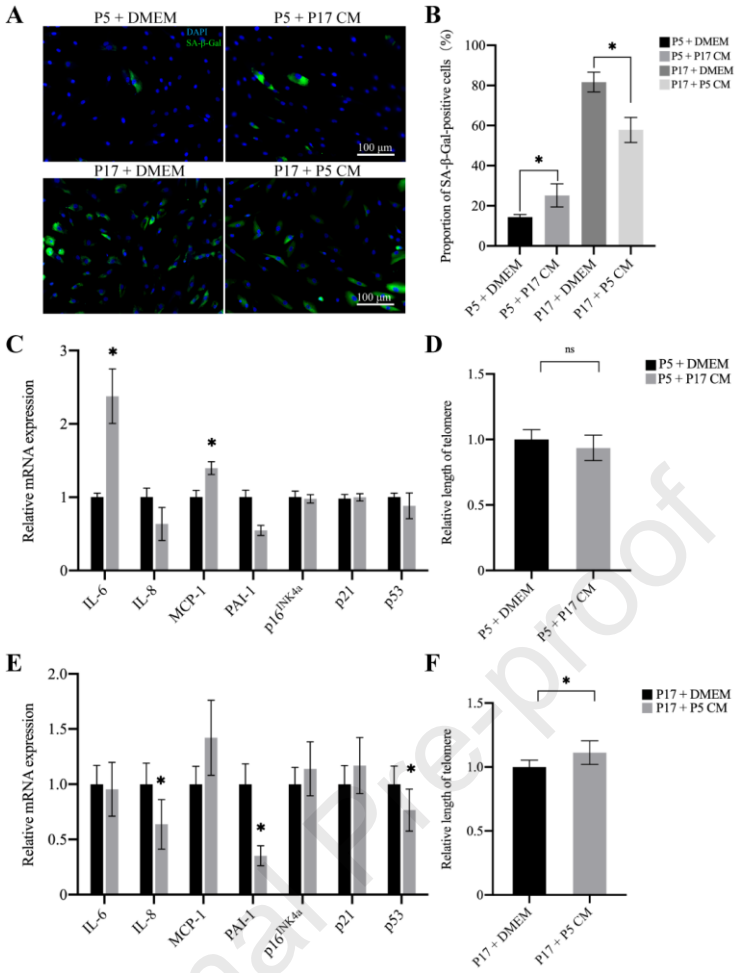

Fig. 2. Endocrine effects of young and senescent hMSCs on cellular senescence.
(A) Representative images of senescent hMSCs, as detected using SA-β-Gal staining. Scale bar: 100 μm. **(B)** Quantification of senescent hMSCs (n = 12, $^{*}p < 0.05$). **(C)** Expression of senescence-associated genes in P5 cells analyzed 96 h after DMEM or P17 CM treatment. **(D)** Relative telomere lengths in DMEM- and P17 CM-treated P5 cells were determined using RT-qPCR. Data are normalized against the values for the DMEM-treated group. Data are presented as means ± SD (n = 4, $^{*}p < 0.05$). **(E)** Expression of senescence-associated genes in P17 cells analyzed 96 h after DMEM or P5 CM treatment. **(F)** Relative telomere lengths in DMEM- and P17 CM-treated P5 cells were determined using RT-qPCR. Data are normalized against the values for the DMEM-treated group. Data are presented as means ± SD (n = 4, $^{*}p < 0.05$).

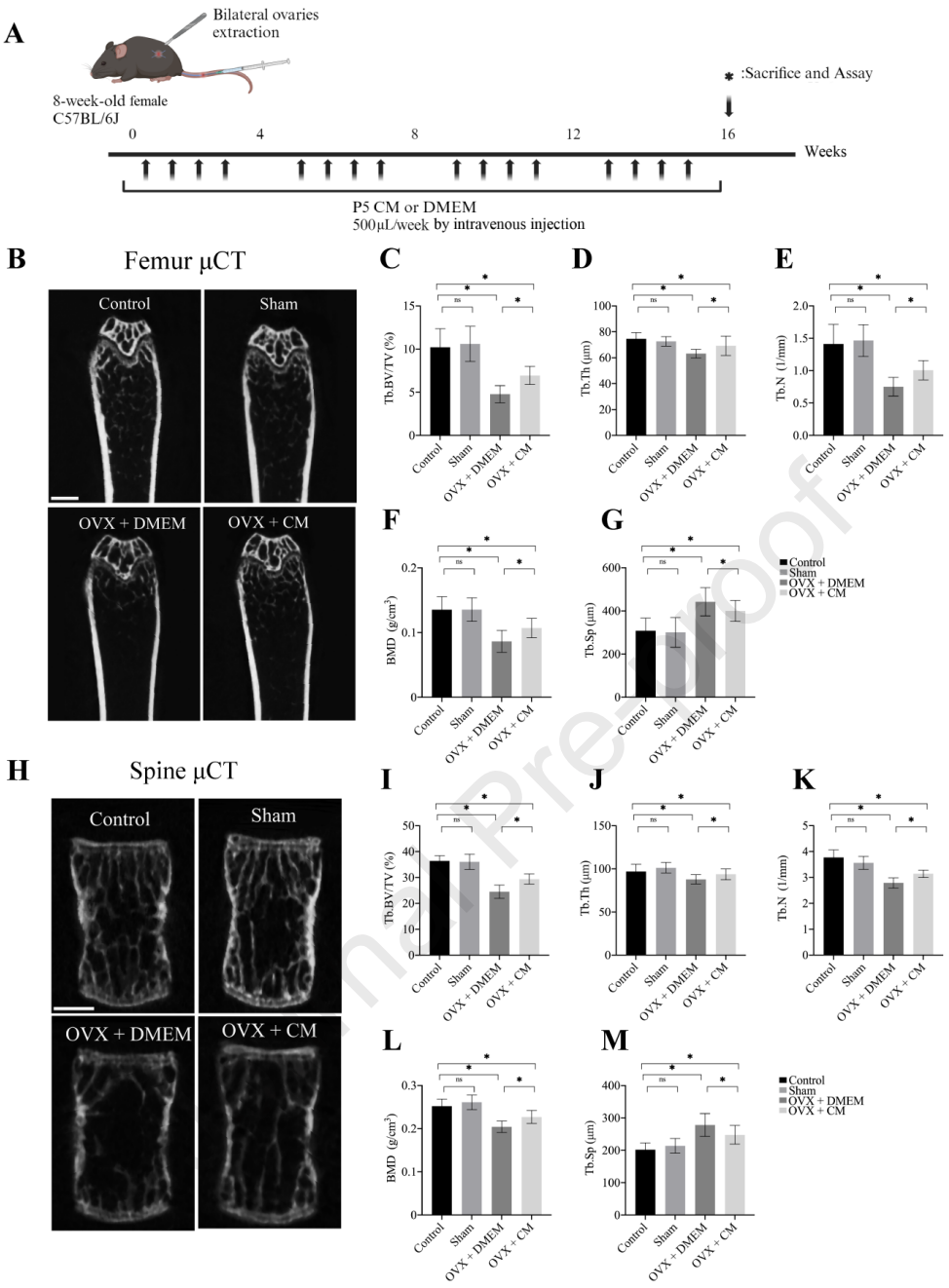

Fig. 3. Conditioned medium of hMSCs (hMSCs-CM) alleviates the symptoms of osteoporosis in mice. (A) Timeline of the vivo experiment. Nine-week-old C57BL/6 mice were randomly divided into four groups: Control, Sham, OVX treated with DMEM (OVX + DMEM), and OVX treated with CM (OVX + CM), and then sacrificed 4 months post-injection. **(B)** Representative μCT images of the femur from Control, Sham, OVX treated with DMEM, and OVX treated with CM mice. Scale bar: 1 mm. **(C-G)** Quantification of the femoral trabecular bone microarchitecture (n = 10, $^{*}p < 0.05$). Tb.BV/TV: trabecular bone fraction; Tb.Th: trabecular thickness; Tb.N: trabecular number; BMD: bone mineral density; Tb.Sp: trabecular separation. **(H)** Representative μCT images of L5. Scale bar: 1 mm. **(I-M)** Quantification of the lumbar trabecular bone microarchitecture. **(I)** Tb.BV/TV. **(J)** Tb.Th. **(K)** Tb.N. **(L)** BMD. **(M)** Tb.Sp (n = 10, $^{*}p < 0.05$).

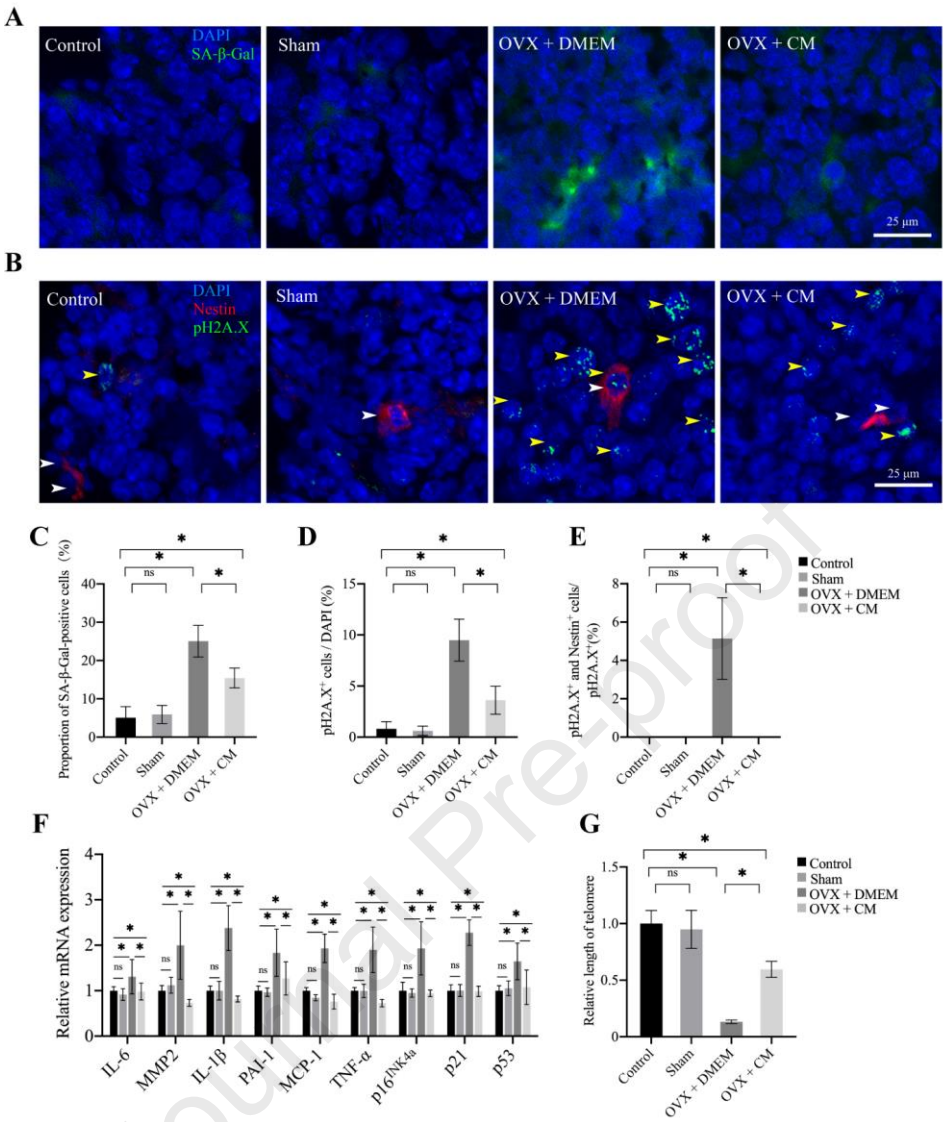

Fig. 4. hMSCs-CM protects mesenchymal stem cells during cellular senescence. (A) Cellular senescence of the distal femur was assessed using immunofluorescence of SA-β-gal-positive cells (green) and DAPI (blue). Scale bar: 25 μm. **(B)** The expression of Nestin (red) in mesenchymal stem cells and the expression of pH2A.X (green) was confirmed by double staining. White arrow, bone marrow MSCs that are not positive to Nestin, yellow arrow, senescent cells that are positive to pH2A.X. Scale bar: 25 μm. **(C)** Percentage of SA-β-Gal-positive cells in the bone microenvironment of the distal femur. **(D)** Percentage of pH2A.X-positive cells in the bone microenvironment of the distal femur. **(E)** Percentage of pH2A.X and Nestin double-positive cells ($n = 10$, $^{*}p < 0.05$). All data are presented as mean ± standard deviation and were analyzed by two independent examiners blinded to the study. **(F)** Expression of genes in the distal femur following a 4-month treatment with CM. Expression levels of *IL-6*, *MMP2*, *IL-1β*, *PAI-1*, *MCP-1*, and *TGF-α*, which are senescence-associated secretory phenotype (SASP) secreted by senescent cells, as well as of $p16^{INK4a}$, p21, and p53, which are associated in cellular senescence, were upregulated in the OVX + DMEM group but downregulated in the OVX + CM group. **(G)** Relative telomere length was analyzed according to Cawthon's method ($n = 4$, $^{*}p < 0.05$).

Highlights

- Paracrine effects of young and senescent hMSCs exerted opposing effects on cellular senescence.
- Postmenopausal osteoporotic mice showed senescent phenotypes represented by increased expression of SASP after ovariectomy.
- hMSCs-derived CM protected BMMSC from entering a senescent state.

Declaration of interests

☒ The authors declare that they have no known competing financial interests or personal relationships that could have appeared to influence the work reported in this paper.

☐The authors declare the following financial interests/personal relationships which may be considered as potential competing interests: